ARTICLE

The intrinsic effect of cofeeding water on the formation of active/deactivating species in the methanol-to-hydrocarbons reaction on a ZSM-5 zeolite

Received 00th January 20xx,
Accepted 00th January 20xx

José Valecillos,*[a] Gorka Elordi,[a] Andrés T. Aguayo,[a] Pedro Castaño*[a,b]

Water is formed and added in the conversion of methanol-to-hydrocarbons, slowing down both the reaction and deactivation rates. This work aims to clarify the selective nature of water quenching on a ZSM-5 zeolite catalyst in terms of (1) reaction/deactivation using an integral reactor (full range of conversions) and (2) rate of formation/growth of deactivating species using two FTIR and UV-vis in situ differential reactors (conversions lower than 0.15). Our approach assesses the effect of water at comparable conversion conditions while characterizing in detail the products and intermediates of reaction (by online and in situ analysis, and extraction measurements). The results obtained prove, in an unbiased way, that water quenches more selectively deactivation over reaction at intermediate amounts of added water (water/methanol = 0.11 g g^{-1}). On the other hand, in situ FTIR spectroscopy evidences that cofeeding water sweeps the retained species from the silanol sites and favors the formation of olefins as retained species, while in situ UV-vis spectroscopy proves that the rate of formation/growth of discrete retained species drop by the addition of water and the degree of this decline is severer for coke than for coke precursors or active species.

Introduction

The acid-catalyzed methanol-to-hydrocarbons (MTH) reaction is the basis for the development of the methanol-to-gasoline (MTG), methanol-to-olefins (MTO), methanol-to-propylene (MTP), and methanol-to-aromatics (MTA) process technologies. The MTH reaction is very versatile as it can be tuned for responding to various market demands, for example, using ZSM-5 zeolite catalysts for the MTG and MTA processes, SAPO-34 catalysts for the MTO process, and stabilized ZSM-5 catalysts for the MTP process.[1,2] The mechanism of methanol/dimethyl ether transformation on ZSM-5 or SAPO-34 catalysts have been extensively studied in the literature.[3–9] The most extended criteria is the formation of methoxy species, followed by C-C bond formation trough methyl acetate and formic acid,[10,11] consecutive methylation-oligomerization, cracking, cyclization and hydrogen transfer of olefins leading to the formation of the hydrocarbon pool species adsorbed/retained in the catalyst.[12–15] The initial formation of the hydrocarbon pool is the autocatalytic period, while its degradation corresponds to the deactivation period: formation and growth of less active or deactivating species, namely coke, on the catalytic surface.

Water is an important component of the MTH reaction. Water is formed in the dehydration of methanol to form dimethyl ether and it is cofed as a common practice in the MTO and MTG process technologies up to approximately 30-50 wt%.[16–18] The positive outcomes of this practice are to facilitate the heat transfer (very exothermic reactions) and to better control the reaction activity and selectivity. However, water may cause the loss of acid sites leading to irreversible catalyst deactivation.[19] At a more fundamental level, water displaces the dehydration equilibrium (2 $CH_3OH \leftrightarrows CH_3OCH_3 + H_2O$) while preventing both the progress of the main reaction, and the formation of highly developed coke.[20] This is evident by comparing the coking rate of methanol (more water in the reaction medium) with that of dimethyl ether as reactant.[21] Several works have focused on understanding the effect of cofeeding water with methanol in the MTH reaction. Most of these works acknowledge that cofeeding water in the MTH reaction increases light olefins selectivity,[22–24] and decreases coke formation and therefore prolongs catalyst lifetime.[22,23,25,26] Chen et al.[27] demonstrated that traces of water effectively accelerate the reactions affecting the hydrocarbon pool during MTH reaction. However, as the amount of water in the reaction medium increases, it attenuates the adsorption capacity of acid sites rather than affecting the equilibrium or the kinetics.[28,29] When analyzing the distribution of light olefins in more detail, some authors[25,30,31] observed that the ethylene selectivity increases more than that of propylene when cofeeding water, while the authors of another work[32] observed that the ethylene selectivity decreases and the propylene selectivity increases when cofeeding water. However, when the observations are made from experiments at incomplete conversion, Möller et al.[33] observed that cofeeding water has no direct effect on products selectivity and the differences they observed in products selectivity are due to the decrease in the conversion (evidenced when plotting selectivity vs conversion). The works of Ghavipour el al.[25] and Möller et al.[33] also made evident that cofeeding water decreases the progress of the reaction indicated by the decrease in the conversion of methanol, which is usually not observed in other works because the experiments

[a] Department of Chemical Engineering, University of the Basque Country (UPV/EHU) P.O. Box 644, Bilbao, 48080 Spain. Email: jose.valecillos@ehu.eus, pedro.castano@ehu.eus
[b] Multiscale Reaction Engineering KAUST Catalysis Center (KCC), King Abdullah University of Science and Technology (KAUST), Thuwal, 23955-6900 Saudi Arabia. Email: pedro.castano@kaust.edu.sa

Electronic Supplementary Information (ESI) available: [details of any supplementary information available should be included here]. See DOI: 10.1039/x0xx00000x

have been performed at conditions at which the oxygenates are fully converted.

Gayubo et al.[19,26] demonstrated that cofeeding water decreases the coking rate, and this effect can be severer at high pressures.[34] Likewise, Aguayo et al.[35] observed less catalyst deactivation in a fluidized-bed reactor in comparison with a fixed-bed reactor due to the improved efficiency of formed water to attenuate coke formation. In line with this and from a more fundamental perspective, De Wispelaere et al.[36] used *in-situ* UV-vis micro-spectroscopy and confocal florescence microscopy and proved that cofed water affects the spatial distribution of active and deactivating species across the crystals of SAPO-34. This effect turns out to be decisive in prolonging the catalyst lifetime. However, Gil-Coba et al.[32] observed no significant changes in the coke content after 5 h on stream, further commenting that the water concentration in the feed does not really affect coke formation after 30 min on stream. Qi et al.[37] observed a similar behavior for SAPO-34 catalysts, concluding that the effect of cofeeding water on attenuating coke deposition weakens gradually with increasing times on stream. Other works,[22,23] giving no experimental measurements of the coke content, have hypothesized that cofeeding water decreases coke formation and therefore attenuates catalyst deactivation (their actual observation). To add more to the controversy, another recent work[38] have indicated that water indeed promotes coking. This deduction was proved by the use of a selective membrane to remove water from the reaction medium, which happens to extend the catalyst lifetime.

Regardless of the discrepancies in the observations of these works, all the authors agree that the cofed water molecules compete with reactants and products for adsorption on acid sites. Indeed, some authors[32,39] have studied the competitive adsorption between water and methanol, ethylene, propylene or 1-butylene by carrying out experimental or theoretical studies, leading to confirm that water partially suppresses the adsorption of these species and inhibits their reactions. The discrepancies in the experimental observations may be due to different criteria in the comparison. Two inadequate criteria are: (i) replacing water by an inert without keeping the same methanol partial pressure and space time because the accessible number of acid sites will change,[33,36] and (ii) using an excess of catalyst in an integral reactor that gives way to complete initial conversions, because this is not an adequate procedure for catalytic performance tests.[40–42] The effect of water should be isolated by comparing the catalytic performance at the same level of (not full) conversions for experiments having different acid site loadings (space times) or different water content, because both effects can lead to similar observations.

In this work, we have isolated the intrinsic effect of water in the deactivation mechanism, grounding the comparison on similar conversion levels. The study was carried out using three reactors: fixed bed for kinetic/deactivation evaluation in the full range of conversions; and two *in-situ* spectroscopic cells for following up the formation of retained species and the structure of the catalytic surface. We combine a detailed product analysis in the three reactors with a detailed characterization of the hydrocarbon pool species (by extraction and *in-situ* spectroscopy). The testing conditions were such that the irreversible catalyst deactivation caused by dealumination is minimal.[19] The thermogravimetric temperature-programmed desorption and oxidation (TPD and TPO) were used to characterize both the active and deactivating species in detail. The dynamics of hydrocarbon pool species followed by extraction, TPO-TPD and *in-situ* spectroscopic measurements were correlated with the dynamics of the product distribution in order to better assess the impact of water on the evolution of reaction intermediates and on the reaction-deactivation pathways.

Experimental

Catalyst preparation and characterization

We prepared a ZSM-5 zeolite by modifying a commercial NH_4ZSM-5 zeolite (Zeolyst International, CBV8014, SiO_2/Al_2O_3 molar ratio = 80) first by calcination (550 ºC for 3 h) and then by $ZnCl_2$ ion exchange as described in a previous publication.[43] Zn modified ZSM-5 zeolites are known to improve the aromatic selectivity when using Zn precursor such as sulfate, acetate or nitrate.[44,45] However, our previous results[43] together with the one of Bi et al.[46] indicate that $ZnCl_2$ modified ZSM-5 zeolite favors the formation of light olefins and slows down the deactivation. The results are reasoned on the significant loss of medium-strength Brønsted acid sites and generation of Lewis acid sites, affecting the performance of the cyclization and hydrogen transfer reactions while promoting the cracking reactions to yield light hydrocarbons.[43,46] In summary, the $ZnCl_2$ modification caused:[43] (i) a decrease in the specific surface of micropores; (ii) decrease in the total acidity determined by NH_3-TPD, decreasing the concentration of strong-strength acid sites while increasing the concentration of medium-strength acid sites; (iii) significant increase in the concentration of Lewis acid sites at the expense of decreasing the concentration of Brønsted acid sites. The balanced catalyst properties in terms of the higher concentration of medium-strength acid sites and equilibrium of Lewis and Brønsted acidities gave an improved performance for the MTH reaction in terms of prolonging the catalyst lifetime. On top, the reaction and deactivation pathways investigated in this work using the indicated catalyst can be considered characteristic of the ZSM-5 zeolite performance.

The modified ZSM-5 zeolite was mixed with 30 wt% of pseudo-boehmite and 20 wt% of α-alumina, followed by drying at room temperature for 24 h and at 110 ºC for 24 h, crushing and sieving at 0.125-0.300 mm, and calcining at 550 ºC for 3 h. We characterized the zeolite and the catalyst by using conventional techniques,[43] including: X-ray photoelectron spectroscopy (XPS), x-ray diffraction (XRD), N_2 physisorption, NH_3 adsorption and temperature-programmed desorption (NH_3-TPD), Fourier-transform (FTIR) spectroscopy, and pyridine adsorption monitored with FTIR spectroscopy.

We characterized the spent catalysts by using temperature-programmed desorption (TPD) and oxidation (TPO) and extraction of retained soluble species. We performed the TPD-TPO measurements in a thermobalance (TA Instruments, Q5000) following this procedure: (i) outgassing ~15 mg of sample at 200 °C for 20 min in N_2 flow; (ii) heating at 10 °C min^{-1} in 50 cm^3 min^{-1} of N_2 up to 550 °C and holding for 1 h; (iii) cooling down to 200 °C and switching the flow to air at 50 cm^3 min^{-1}; and (iv) heating at 10 °C min^{-1} up to 550 °C and holding for 90 min. The experimental data allowed quantifying the coke content. The extraction of soluble retained species is based on the standard procedure developed by Guisnet and coworkers and adapted as described in a previous publication.[43] The experimental procedure consisted of (i) treating ~10 mg of sample in HF (Merck, 40%) with a sample/HF ratio of 10 cm^3 g^{-1} in a Teflon container for 1 h; (ii) neutralizing with a NaOH (Panreac, pure) solution; (iii) adding 3 cm^3 of dichloromethane (Sigma-Aldrich, 99.8%) and shaking for 1 min; (iv) allowing for the separation the organic and aqueous phases for 2 h and recovering the organic phase for analysis. We analyzed the organic phase in a gas chromatograph coupled with a mass spectrometer (Shimadzu, GCMS-QP2010S).

Reaction tests in a fixed-bed reactor

We investigated the main kinetic tests for the MTH reaction in a conventional fixed-bed reactor at constant conditions and tested different water-to-methanol weight ratios in the feed from 0 (reference experiment) to 1 by feeding pure methanol or methanol-water mixtures. The constant conditions for the MTH reaction were temperature (T) = 400 ºC, total pressure (P_T) = 1.85 bar, methanol partial pressure (P_{M0}) = 0.610 bar, methanol flowrate (F_{M0}) = 0.1 mol h^{-1}, methanol concentration (%Y_{M0}) = 33 mol%, catalyst weight (W) = 0.1 g, space time (W/F_{M0}) = 1 g h mol^{-1}. Afterward, we selected specific experiments for studying the deactivation kinetic by carrying the MTH reaction experiments until we observed high levels of catalyst deactivation, which is indicated by the increase of reactants and decrease of products. The reaction setup was described in detail in a previous publication.[43] Briefly, the reactor is a stainless-steel tube (inner diameter = 9 mm) with fixed-bed arrangement of 6 cm^3 consisting of a mixture of SiC (VWR Chemicals, < 0.105 mm) and catalyst sample (0.1 g), which is inside of a hot box kept at 200 ºC to prevent the condensation of the products for analysis in gas-vapor phase. The feed consisted of liquid pure methanol or methanol-water mixtures pumped at 0.1 mol h^{-1} of methanol diluted with adjusted flowrates of He in order to keep the same methanol concentration (water replaces He as the diluent in the experiments with water co-feed). The products analysis was carried out online using a micro-gas chromatograph (Varian, CP4900) with a thermal conductivity detector and three column channels for simultaneous analysis: (i) Molesieve 5A (fumed SiO_2, packed length = 8 m, column temperature = 45 ºC, column injection temperature = 65 ºC, column pressure = 26 psi) for separation of N_2, O_2, CO and CH_4; (ii) PoraPLOT Q (packed length = 10 m, column temperature = 80 ºC, column injection temperature = 80 ºC, column pressure = 26 psi) for separation of C_1-C_4 hydrocarbons and oxygenates; and (iii) CP-Sil 5 CB (packed length = 10 m, column temperature = 80 ºC, column injection temperature = 80 ºC, column pressure = 26 psi) for separation of C_4-C_{10} hydrocarbons a oxygenates. We calculated the carbon-based conversion (X) assuming that all the identified oxygenates (methanol and dimethyl ether) are reactants:

$$X = \frac{F_{M0} - F_M}{F_{M0}} = 1 - Y_M \quad (1)$$

Where F_{M0} is the carbon-based molar flowrate of oxygenates in the feed, F_M is the carbon-based molar flowrate of oxygenates in the products and Y_M is the carbon-based yield of oxygenates in the products. We calculated the carbon-based yield of a product i (Y_i) or the carbon-based selectivity of a product i (S_i) as follows:

$$Y_i = \frac{F_i}{F_{M0}} \quad (2)$$

$$S_i = \frac{F_i}{F_{M0} - F_M} = \frac{Y_i}{X} \quad (3)$$

Where F_i is the carbon-based molar flowrate of product i. We fitted the experimental datasets by using the simple fitting models described in the Supporting Information, in which the coadsorption of water is taken into account.

Reaction tests in in situ cell reactors

We performed the MTH reaction in in situ cell reactors at constant conditions and tested various water-to-methanol weight ratios in the feed from 0 (reference experiment) to 1 with the purpose of monitoring the changes in the catalyst surface by FTIR or UV-vis spectroscopies. The conditions for the MTH reaction were temperature (T) = 400 ºC, total pressure (P_T) = 1 bar, methanol partial pressure (P_{M0}) = 0.012 bar, methanol flowrate (F_{M0}) = 0.1 mol h^{-1}, methanol concentration (%Y_{M0}) = 1.4 mol%, catalyst weight (W) = 0.012 g, space time (W/F_{M0}) = 1 g h mol^{-1}. We used two commercial spectroscopic chambers as cell reactors: a Specac high temperature high pressure (HTHP) cell for a FTIR spectrometer (Thermo Scientific, Nicolet 6700) and a Linkam cell (THMS600) for a UV-vis spectrometer (Jasco, V-780) with a special compartment (Jasco, ARN-915i) for the cell. The feed consisted of N_2 containing methanol vapor or methanol and water vapors keeping constant the methanol concentration (water vapor replaces N_2 in the experiments with water co-feed). We obtained these vapors by flowing N_2 through saturator vessels containing methanol or water, and we calculated the methanol and water concentrations using the equilibrium data at room temperature. We analyzed the gas- or vapor-phase products by using a mass spectrometer (Pfeiffer Vacuum, Omnistar GSD 320 O Series) continuously measuring the m/z signals of 16, 18, 27, 29, 31, 41, 43, 45, 55, 56, 57, 78 and 91. We performed the *in-situ* UV-vis spectroscopy experiments in continuous mode for a total time on stream of 4 h and collecting spectra every 35 s. We performed the *in-situ* FTIR experiments in discontinuous mode by pulses of reaction.

The first pulse consisted of feeding pure methanol or a methanol-water mixture for 1 min followed by flushing with N_2 for 1 h and collection of a spectrum. For the subsequent pulses, we fed pure methanol or a methanol-water mixture for increasing times (1-32 min) with flushing periods of 1 h in-between pulses and collection of spectra after flushing. The reason for operating in discontinuous mode relies on the strong interference of water in the FTIR spectra, which becomes significant when co-feeding water.

Results

Fixed-bed reactor

The experiments carried out in the fixed-bed reactor allowed to assess the effect of cofeeding water on the MTH performance on the ZSM-5 catalyst in a while range of conversions (integral reactor) with a detailed characterization of products. At the same time, this effect can be compared with that of changing the space time. Additional ex situ analyses of the spent catalysts allowed quantifying and studying the nature of the retained species in each experiment. The following subsections show the results for the study of the kinetic and deactivation performance in a fixed-bed reactor and the ex situ analysis of retained species.

Kinetic and deactivation performance. Figure 1 shows the initial conversion of oxygenates (measured at 10 min on stream) for experiments with different water-to-methanol ratios (F_{W0}/F_{M0}) in the feed, and different space times (in this case the space velocity as F_{M0}/W). As seen, the conversion decreases with increasing water-to-methanol ratios in the feed or decreasing space times, as reported in other works.[26,33,43,47] This indicates that the effect of cofeeding water in changing the extent of the reaction is similar to that of decreasing the amount of available acid sites for the reaction by tuning the catalyst weight for changing the space time. The decrease in the conversion with increasing water-to-methanol ratios in the feed is attributed to the adsorption of cofed water on acid sites preventing the adsorption of reactants and products. This causes a decrease in the concentrations of adsorbed reactant species leading to decrease the reaction rates. Based on these assumptions, we used Equation S5 to fit the experimental dataset of Figure 1a and 1b, and we obtained a very high goodness of fit (R^2 = 0.9926-0.9948) with k_1 = 0.0587 h^{-1}, k_2 = 10.9 h^{-1} for both cases and K_W = 6.13 when cofeeding water. This indicates that the effect of cofeeding water can be satisfactorily explained by the coadsorption of water, which makes a portion of the acid sites unavailable for the reaction. The portion of unavailable acid sites is proportional (by K_W) to the water-to-methanol ratio in the feed.

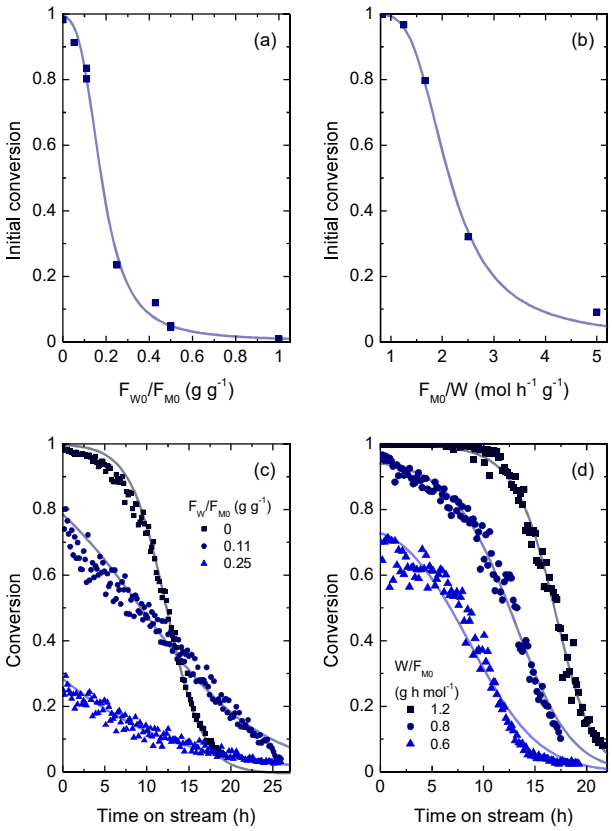

Figure 1. Effect of cofeeding water (variation of F_{W0}/F_{M0}) on (a) the initial conversion and (c) deactivation profiles, and effect of space time (variation of W/F_{M0}) on (b) the initial conversion and (d) deactivation profiles for the MTH reaction. Conditions for (a) and (c): T = 400 ºC, P_{M0} = 0.61, W/F_{M0} = 1 g h mol^{-1}, F_{W0}/F_{M0} = 0-0.5. Conditions for (b) and (d): T = 400 ºC, P_{M0} = 1.57 bar, W/F_{M0} = 0.2-1.2 g h mol^{-1}, F_{W0}/F_{M0} = 0.

From these exploratory experiments, we chose the experiments with water-to-methanol ratios in the feed of 0, 0.11 and 0.25 (Figure 1c) and space times of 0.6, 0.8 and 1.2 g h mol^{-1} (Figure 1d) to study the deactivation performance. As seen, all the experiments show catalyst deactivation indicated by the decrease of the conversion with increasing times on stream. Cofeeding water slows down the decrease of the conversion (deactivation rate), which prolongs the catalyst lifetime. On the other hand, changing the space time does not affect the decrease of the conversion, and the catalyst lifetime is shortened as the number of acid sites decreases. We proved this by fitting to Equation S7 the experimental dataset of Figure 1c and 1d, and we found that k_d remains constant regardless of changing the space time (as expected) or cofeeding water. However, the additional attenuation effect on catalyst deactivation provoked by cofeeding water can be explained by using an attenuation coefficient (k_W) as described by Gayubo et al.[26] and further described in the Supporting Information, and in this case we found little dependency on the water-to-methanol ratio (n = 0.1 for fitting the experimental dataset of Figure 1c to Equation S7). Using the fitting models, we found that the estimated catalyst lifetimes (defined as the time on stream at which the conversion decreases 90% of its initial value) are 17.3, 26.7 and 26.8 h for the experiments with water-

to-methanol ratios in the feed of 0, 0.11 and 0.25, respectively. In contrast, the catalyst lifetime decreases from 20.1 to 15.2 h when the space time decreases from 1.2 to 0.6 g h mol^{-1}. These comparisons confirm the additional role of cofeeding water on attenuating catalyst deactivation regardless of the similarities of cofeeding water and changing the space time in decreasing the extent of the reaction.

The analysis of the product distribution obtained from the study at initial conversions in terms of product yields evidences similarities between both experimental scenarios, those of co-feeding water (Figures S1a and S2a) and changing the space time (Figure S1b and S2b). Figure 2 shows the product distribution in terms of the product selectivity against conversion for both experimental scenarios. As seen, the selectivity of light olefins (LO), including ethylene (E) and propylene (P), and light gases (LG) decreases while that of light paraffins (LP), heavy aliphatics (HA) and aromatics (BTX) increases with increasing conversions for both experimental scenarios. However, the decreasing trend in the selectivity of aromatics changes at low conversions for the experimental scenario of cofeeding water (at high water-to-methanol ratios in the feed according to Figure 1a), indicating that the selectivity of aromatics starts to increase at low conversions (< 0.2). Despite of this change, we observed an expected behavior for the selectivity of products, indicating that light olefins undergo methylation/oligomerization and hydrogen transfer reactions at high conversions (similar to what happens with the increase of the space time). When we take into consideration the experimental scenarios, it becomes evident that the most significant effect of cofeeding water on the product distribution consists of tuning the conversion, which implicates changes in the product distribution. Möller et al.[33] attributed the differences observed in the product selectivity to the change in the conversion provoked by cofeeding water in the MTH reaction on a HZSM-5 catalyst. Our results also confirm that water promotes only insignificant changes in the selectivity when the values are compared in the same conversion range. We were able to observe an improvement in the propylene selectivity in the whole conversion range of 0.4-1.0 as shown in Figure S3, in agreement with other works.[25,30,31] However, this improvement is marginal at similar conversion values.

Ex situ analysis of retained species. To complete our product analysis, we analyzed the remaining species in the spent catalyst of each experiment by carrying out TPD-TPO measurements and extraction of soluble species. The TPD profiles of the spent catalysts at variable water-to-methanol ratios in the feed (Figure 3a) and at variable space time (Figure 3b) show essentially one peak at 526 ºC similar in intensity for all the experiments, which is associated with the degradation or decomposition of retained species and coke.[43,48] Curiously, the intensity of this peak decreases as more water is added in the feed, whereas it remains practically constant for the spent catalysts at variable space times. This indicates that cofeeding water allows an easier diffusion of coke precursors throughout and out of the zeolite.[19] Likewise, the amount of retained soluble species (in this work: tetra-, penta- and hexamethylbenzenes) was very low because of the severe catalyst deactivation, and we found that the relative abundance of these species decreases with increasing water-to-methanol ratios in the feed (Figure S4a). These species can be correlated with the TPD measurements (Figure S4b), indicating that most of the TPD species are related to the desorption or decomposition of soluble species.

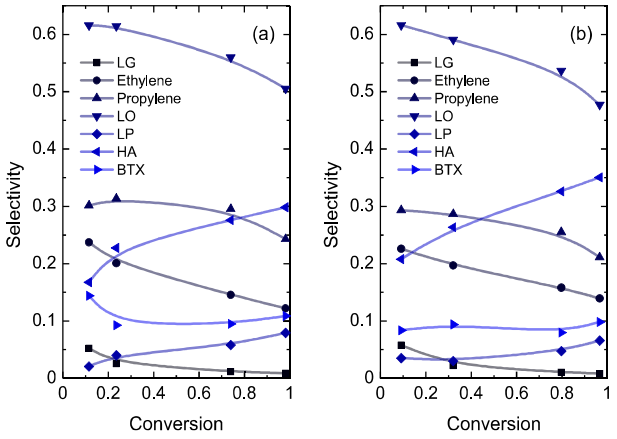

Figure 2. Effect of (a) cofeeding water (variation of F_{W0}/F_{M0}) and (b) changing the space time (variation of W/F_{M0}) on the initial selectivity of products against conversions for the MTH reaction: light gas (LG), ethylene (E), propylene (P), light olefins (LO), light paraffins (LP), heavy aliphatics (HA) and aromatics (BTX). Conditions: T = 400 ºC, P_{M0} = 0.28 bar, W/F_{M0} = 1 g h mol^{-1}. Conditions for (a): T = 400 ºC, P_{M0} = 0.61, W/F_{M0} = 1 g h mol^{-1}, F_{W0}/F_{M0} = 0-0.5. Conditions for (b): T = 400 ºC, P_{M0} = 1.57 bar, W/F_{M0} = 0.2-1.2 g h mol^{-1}, F_{W0}/F_{M0} = 0.

The corresponding TPO profiles for each experimental scenario show only one peak centered at 546 ºC associated with the combustion of coke.[43] The intensity of the TPO peak decreases as the water-to-methanol ratio in the feed increases (Figure 3a) or as the space time decreases (Figure 3b).Figure 4 shows the coke content calculated from the TPO profiles as a function of the average conversion for both experimental scenarios. The calculation of the average conversion is based on Figures 1c and 1d and consists of integrating the conversion curve for each experiment and dividing by the corresponding time on stream range. Thus, we obtain the relative amount of converted oxygenates in each experiment. This amount expectedly increases with increasing space time (more catalyst, more conversion) and decreasing water-to-methanol ratio in the feed (cofed water attenuates the conversion of oxygenates into hydrocarbons). Consequently, the average coke content decreases as the average relative amount of converted oxygenates decreases for a specific experiment (more converted carbon, more coke). As seem, the dataset of both experimental scenarios can be described by a common curve, making the coke content a function of the amount of converted oxygenates. This indicates that the coke formation is similar for both experimental scenarios and independent of controlling the amount of converted oxygenates by either cofeeding water or changing the space time; it solely depends on the conversion levels.

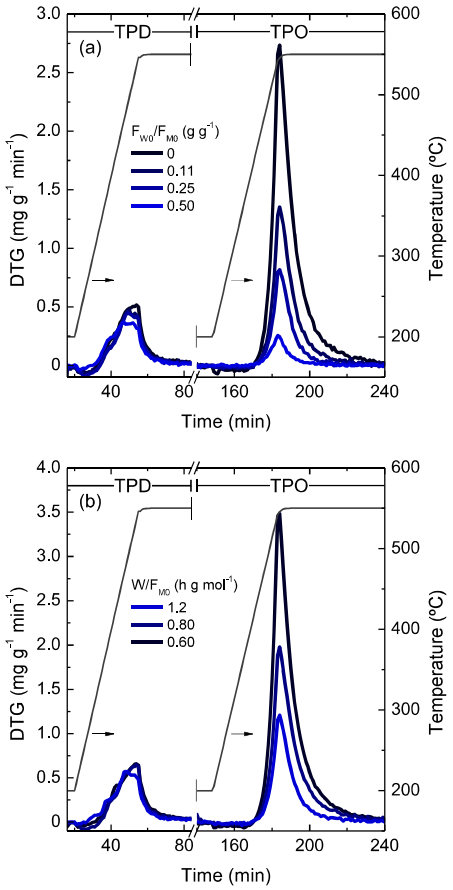

Figure 3. TPD-TPO profiles of the spent catalyst after the MTH reaction at different (a) water-to-methanol (F_{W0}/F_{M0}) ratios in the feed and (b) space times (W/F_{M0}).

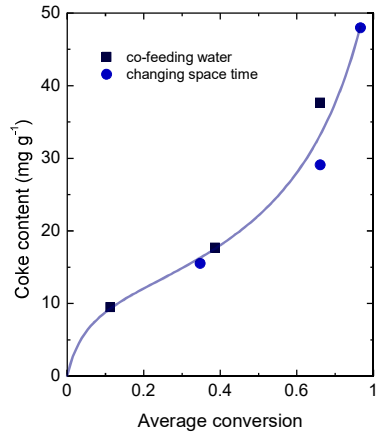

Figure 4. Coke content as a function of the average conversion for the experimental scenarios of cofeeding water (variation of F_{W0}/F_{M0}) and changing the space time (variation of W/F_{M0}).

In situ cell reactors

The primary kinetic observations in the fixed-bed reactor indicate that cofeeding water decreases the formation of coke and retained soluble species in similarity to the effect of changing the space time that controls the extent of the reaction. Thus, we further analyzed the in situ formation of retained species detected by FTIR or UV-vis spectroscopies under MTH reaction conditions, with different water-to-methanol ratios in the feed. In these reaction systems, the conversion is lower, and the reaction rates are slower than those observed in the fixed-bed reactor. Therefore, these systems behave as differential reactors, and we analyzed the incipient formation of retained species.

Exposing the catalyst sample to feeds of pure methanol or methanol-water diluted in nitrogen gave rise to different UV-vis or FTIR bands related to the formation and retention of hydrocarbons in the catalyst. Before analyzing the spectroscopic information, we analyzed the conversion and product distribution in the two differential reactors over time on stream for three water-to-methanol ratios in the feed (F_{W0}/F_{M0} = 0, 0.5 and 1) using a mass spectrometer. This analyzer provided us with more limited information than the micro-gas chromatograph, but enough to prove the conversion and other important parameters. Figure S5 shows the evolution with time on stream of the MS signals related to hydrocarbons (m/z = 41, 55, 56, 57, 70 and 91) and oxygenates (m/z = 31 and 45), showing a stable evolution that indicates a steady-state operation. Figure 5 shows the conversion against water-to-methanol ratios in the feed for the experiments in the fixed-bed reactor, and UV-vis and FTIR cell reactors at steady-state conversions (measured at 10 min on stream for the fixed-bed reactor and 300 min on stream for the cell reactors). As seen, conversions are very low due to the use of differential conditions with lower methanol partial pressures in comparison the conditions in the fixed-bed reactor. However, we observe a similar effect in the three reactors: the conversion decreases with increasing water-to-methanol ratios in the feed.

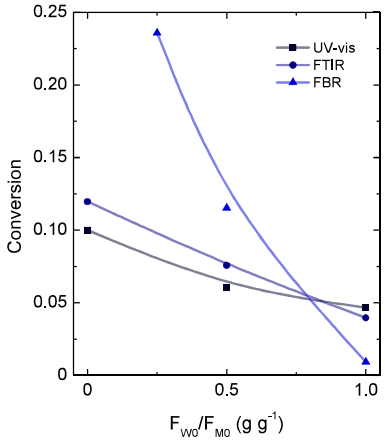

Figure 5. Effect of cofeeding water on the conversion obtained in the fixed-bed reactor (FBR) and FTIR and UV-vis cell reactors. Conditions: T = 400 ºC, P_{M0} = 0.61 bar (FBR) 0.014 bar (FTIR or UV-vis cell reactors), W/F_{M0} = 1 g h mol^{-1}, F_{W0}/F_{M0} = 0-1.

UV-vis spectroscopy. For the set of UV-vis spectra (Figure S6), the most relevant bands are centered at 392-434, 576 and 708 nm respectively corresponding to carbocationic species of monocyclic aromatics, polycyclic aromatics and large polycyclic aromatics.[36,43,49–54] In all spectra, we observe a very fast (in the first 100 s) formation of 288 and 344 nm bands assigned to neutral aromatics and carbocations of monocyclic aromatics

with low number of substituents or monoenyl olefins, respectively. The 344 nm band tend to shift towards 392 and 434 nm, corresponding to the growth of monocyclic aromatic carbocations (increasing number of substituents) or dienyl olefins. This last effect coincides with the formation of 484 and 576 nm bands, assigned to polycyclic aromatics. After 350 s, the retained species on the catalysts enter in a different stage, experimenting a consistent growth, particularly of the 576, 708 and 822 nm bands, with the last two bands assigned to more developed polycyclic aromatics. When comparing the effect of water on the band evolutions, the bands of 344, 392, 576-822 nm seem to be greatly quenched by the presence of water in the feed.

Figure 6 shows the evolution with time on stream of the maximum intensity of these UV-vis bands for the beginning of the reaction. As seen, the 392 nm band is the first to appear and this band gives rise to the 576 and 708 nm bands, indicating that monocyclic aromatics are precursors for polycyclic aromatic species. Cofeeding water delays the initial formation of all the retained species, being dependent on the water-to-methanol ratio in the feed. This can be interpreted by the fact that water affects the equilibrium of the initial methoxy/acetate chemistry,[55] and is competitively adsorbed on acid sites reducing the amount of available sites for the adsorption of reactive species that give rise to the retained species.

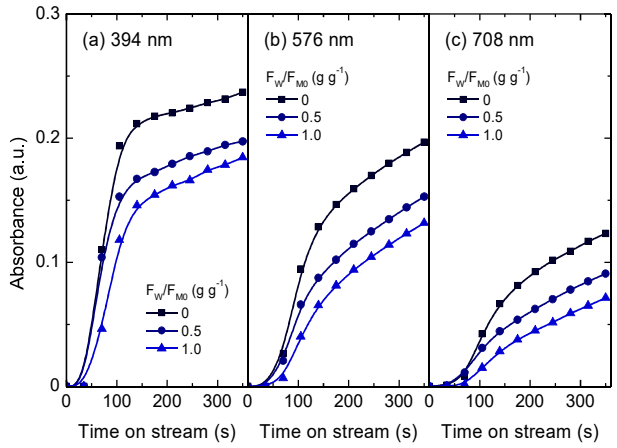

Figure 6. Evolution with time on stream of selected UV-vis bands during the MTH reaction: (a) 394 nm, (b) 576 nm and (c) 708 nm. Conditions: T = 400 ºC, P_{M0} = 0.014 bar, W/F_{M0} = 1 g h mol^{-1}, F_{W0}/F_{M0} = 0-1.

FTIR spectroscopy (retained species). Figure 8 shows the set of FTIR spectra obtained by carrying out discontinuous experiments (by pulses of methanol or methanol-water diluted in nitrogen). It is noteworthy to mention that we carried out additional experiments in continuous mode in the FTIR cell reactor in order to obtain appropriate information of the gas- or vapor-phase products for this system but we observed a strong interference of cofed water on the spectra quality and interpretation. All the experiments show bands corresponding to the stretching vibration of C-H bonds (2850, 2906, 2923 and 2954 cm^{-1}) and C=C bonds (1462, 1570 and 1591 cm^{-1}), and bending vibration of C-H bonds (1377, 1392 and 1481 cm^{-1}).[43] These bands represent the accumulation of different stable retained species in the catalyst, as we obtained each spectrum after outgassing the catalyst sample (all weakly adsorbed species are removed in the outgassing stage). Based on the evolution of the bands and previous publications,[43,53,54,56–60] we infer that the 1377, 1392 and 1591 cm^{-1} bands correspond to carbocationic olefin species adsorbed on acid sites, as they evolve together and are the first ones to appear, and subsequently disappear after prolonged times of exposure giving rise to bands related to other aromatic species (1462 and 1570 cm^{-1}). Thus, olefins are the first formed species as the spectrum after 1 min of exposure only show predominant bands at 1377, 1392 and 1591 cm^{-1}. After successive exposures to methanol or methanol-water pulses, these olefins are converted into aromatic species indicated by the progressive appearance of the 1462, 1481 and 1570 cm^{-1} bands. The addition of water in the feed prolongs the permanence of olefins as predominant retained species while the presence or formation of aromatic species is significantly quenched. Likewise, the intensity of all the bands decreases for the experiments with water cofeed, indicating that the addition of water in the feed attenuates the formation of retained species, particularly that of aromatic species.

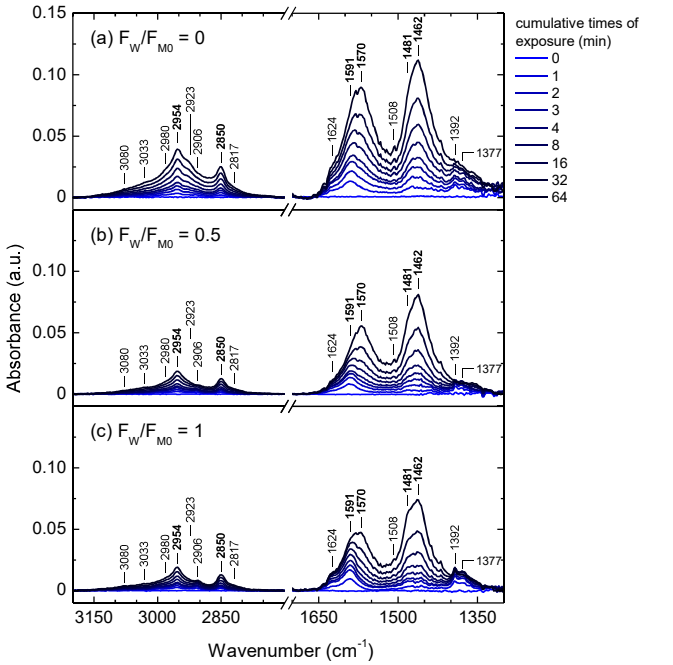

Figure 7. Effect of cofeeding water on the evolution with cumulative time of exposure of FTIR spectra during the MTH reaction with water-to-methanol ratios of (a) 0, (b) 0.5 and (c) 1. Conditions: T = 400 ºC, P_{M0} = 0.014 bar, W/F_{M0} = 1 g h mol^{-1}.

FTIR spectroscopy (acid sites). The FTIR spectra also provide information on the acid sites of the catalyst by inspecting the region of stretching vibrations of O-H bonds (3550-3800 cm^{-1}). Figure 8a depicts the FTIR spectrum in this region at the end of each experiment carried out in the FTIR cell reactor. As seen, all the bands have negative absorbance intensities indicating that the acid sites remain covered by retained species once the reaction is over and after outgassing the catalyst. The Brønsted acid sites (3595 cm^{-1}) are practically covered at the end of each

experiment, while cofeeding water slightly decreases the intensity of the band corresponding to Brønsted acid sites pointing towards less coverage by retained species. The silanol sites (3718 and 3730 cm^{-1}) are strongly covered at the end of the experiment with the pure methanol feed, whereas cofeeding water strongly decreases the absorbance intensities corresponding to silanol sites indicating much less coverage by retained species of these sites with increasing water-to-methanol ratios in the feed. In order to verify the effect of cofed water on acid sites, we carried out an experiment in the FTIR cell reactor consisting of exposing the catalyst sample to a flow of water in nitrogen equivalent to the maximum water flowrate (for a water-to-methanol ratio of 1) for 24 h at the same reaction conditions. Figure 8b shows the spectra obtained before and after exposing the catalyst to water, evidencing that water does not affect the bands related to acid sites at the reaction conditions used in this work. This also verifies that the catalyst does not undergo dealumination by its exposition to water at 400 ºC, as previously reported for even more acidic ZSM-5 catalysts in the MTH reaction with water cofeed.[19]

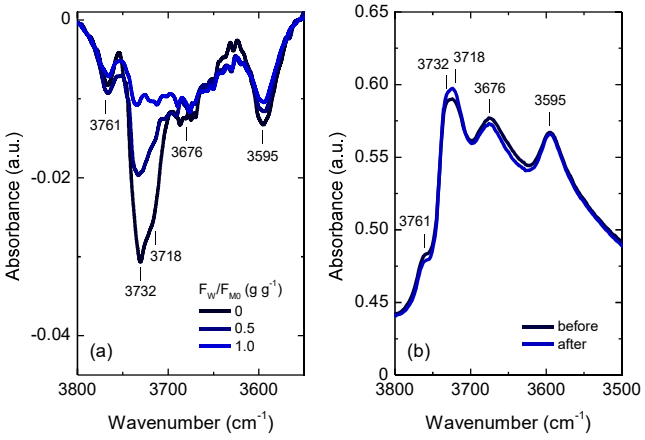

Figure 8. FTIR spectra of the catalyst in the 3500-3800 cm^{-1} region at (a) the end of each experiment with different water-to-methanol ratios in the feed and (b) before and after exposing the catalyst to a flow of water at the reaction conditions. Conditions: T = 400 ºC, P_{M0} = 0.014, W/F_{M0} = 1 g h mol^{-1}, F_{W0}/F_{M0} = 0-1.

We further analyzed the different silanol bands into that of internal silanols (3718 cm^{-1}) and external silanols (3730 cm^{-1}) during the MTH reaction. Figure 9 shows the evolution with times of exposure of these bands with negative absorbance intensities indicating they are covered by retained species. As seen, cofeeding water decreases the levels of absorbance intensities of these bands during the MTH reaction, indicating that cofed water specifically prevents the adsorption of retained species on these sites. The silanol sites are equally affected regardless of their location (internal or external silanol sites). Based on the previous analysis of hydrocarbon species, we infer that aromatic species are preferentially adsorbed on the silanol sites as the formation of these species is greatly quenched by cofeeding water.

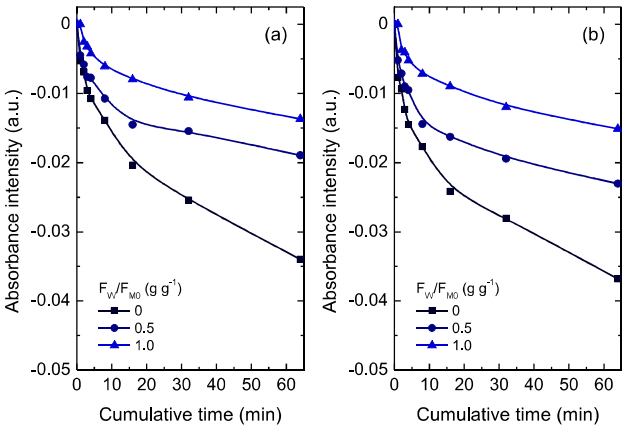

Figure 9. Effect of cofeeding water on the evolution with cumulative times of exposure of silanol FTIR bands during the MTH reaction: (a) 3718 cm^{-1} and (b) 3730 cm^{-1}. Conditions: T = 400 ºC, P_{M0} = 0.014 bar, W/F_{M0} = 1 g h mol^{-1}, F_{W0}/F_{M0} = 0-1.

Discussion

In this work, we compared two experimental scenarios in order to change the water concentration in the reaction medium and at the same time the conversion levels: cofeeding water and changing space time. Our results indicate that there are many similarities in the kinetic behavior of the MTH reaction under both experimental scenarios, whereas the addition of water in the feed attenuates catalyst deactivation. In order to quantify the impact of changing one or another condition, we used simple fitting models that take into consideration the role of added water in the reaction medium.

It is noteworthy to mention that we also considered formed water in an alternative model (Supporting Information). However, the use of a term for formed water leads to a marginal improvement of the fitting (the normalized error slightly decreases) with an additional fitting parameter (Figure S8 and Table S1 in the Supporting Information). Thus, we consider that the model with only the term for cofed water accounting for the attenuation of the reaction rate is optimum since it fits the experimental data quite satisfactorily and requires less fitting parameters. This also evidences that the effects of cofed and formed water on attenuating the reaction rate are different, being that of cofed water more impactful since $K_W >> K_{FW}$ (Table S1 in the Supporting Information), where K_W and K_{FW} are the cofed and formed water adsorption coefficients, respectively.

The deduction of these models is described in the Supporting Information and here we present the two fundamental expressions that describe the kinetic and deactivation of the experimental data shown in Figure 1:

$$(-r) = \frac{dX}{d(W/F_{M0})} = \frac{(1-X)(k_1 + k_2 X)}{1 + K_W R_W} a \qquad (4)$$

$$-\frac{da}{dt} = \frac{k_d}{1 + k_W {R_W}^n} \qquad (5)$$

Where r is the reaction rate, X is the conversion of oxygenates, W/F_{M0} is the space time, k_1 is the kinetic coefficient for the

simplified reaction M → H (where M stands for oxygenates and H for hydrocarbons), k_2 is the kinetic coefficient for the simplified reaction M + H → H, K_W is the cofed water adsorption coefficient, R_W is the water-to-methanol ratio in the feed, a is the activity term, t is the time on stream, k_d is the deactivation coefficient, k_W is the attenuation coefficient for the cofed water and n is an empirical order with respect to R_W in the attenuating effect of cofed water on the catalyst deactivation. Equation 4 essentially describes the reaction rate in steady-state conditions (also used for zero time on stream) based on the conversion of oxygenates, where the term $1 + K_W R_W$ accounts for the attenuation of the reaction rate because of the adsorption of cofed water on acid sites. Likewise, Equation 5 describes the catalyst deactivation by the decrease in the activity term (a) as a function of the time on stream (t), where the term $1 + k_W R_W^n$ accounts for the attenuation in the catalyst deactivation by cofed water. Thus, the attenuated kinetic and deactivation coefficients for each experiment can be defined as:

$$k' = \frac{k_2}{1 + K_W R_W} \quad (6)$$

$$k_d' = \frac{k_d}{1 + k_W {R_W}^n} \quad (7)$$

These attenuated coefficients take into consideration the amount of water that is cofed in each experiment and the assumption that cofed water is practically adsorbed on acid sites. Note that we omitted k_1 in Equation 7 as we obtained that $k_1 << k_2$ from the fittings. For the experiments with variable space time, $1 + K_W R_W = 1$ and $1 + k_W R_W^n = 1$ since $R_W = 0$, and the coefficients are independent of the space time as expected in typical kinetic models.[61] For the experiments with variable water-to-methanol ratio in the feed, $1 + K_W R_W$ and $1 + k_W R_W^n$ are variable for each experiment depending on the water-to-methanol ratio (R_W), and then the effect of cofeeding water can be quantified in terms of these attenuated coefficients. Table 1 shows the attenuated kinetic (k') and deactivation (k_d') coefficients together with the variation with respect to the reference experiment (variable W/F_{M0} or $F_{W0}/F_{M0} = 0$). Both coefficients significantly decrease with the addition of a small amount of water in the feed ($F_{W0}/F_{M0} = 0.11$), whereas further increases in the amount of water in the feed ($F_{W0}/F_{M0} = 0.25$) cause a more relevant decrease in k' than in k_d'. By dividing the variation of k' by that of k_d' for each experiment (k'/k_d' variation), we can measure the relative impact of cofeeding water on the kinetic or deactivation. Cofeeding small amounts of water ($F_{W0}/F_{M0} = 0.11$) give a k'/k_d' variation of 0.903 while increasing amounts of water ($F_{W0}/F_{M0} = 0.25$) give a k'/k_d' variation of 1.30. Thus, low water contents in the feed is beneficial for attenuating the deactivation more than the kinetic of the reaction, whereas high water contents do not favor the attenuation of the deactivation. The observations in the in situ experiments evidenced that the kinetic formation of retained species with the role of being active and deactivating species decreased as more water is cofed.

Table 1. Kinetic and deactivation coefficients of the proposed model in Equations (7)-(8).

Experimental scenario	k'[(a)] (h^{-1})	Variation[(c)] (%)	k_d'[(b)] (h^{-1})	Variation[(c)] (%)	k'/k_d' variation
variable W/F_{M0}	10.8	-	0.0422	-	
$F_{W0}/F_{M0} = 0$	10.8	-	0.0422	-	
$F_{W0}/F_{M0} = 0.11$	6.48	40.2	0.0234	44.5	0.903
$F_{W0}/F_{M0} = 0.25$	4.28	60.5	0.0225	46.5	1.30

(a) k' is the attenuated kinetic coefficient; (b) k_d' is the attenuated deactivation coefficient; (c) the variation is $(x_0 - x)/x_0$, with $x = k'$ or k_d' and x_0 is k' or k_d' of the reference experiment (variable W/F_{M0} or $F_{W0}/F_{M0} = 0$).

These observations lead to conclude that the impact of cofed water on the kinetic and deactivation of the ZSM-5 catalyst in the MTH reaction is mostly because of the water adsorption on acid sites. This phenomenon evidently reduces the amount of available acid sites for the reaction network, being similar to the effect of reducing the amount of available acid sites by lowering the catalyst weight for tuning different space times. However, the key difference between both experimental scenarios is the actual density of acid sites. While the density of acid sites remains practically constant by just changing the catalyst amount in the catalytic bed (only the total amount of acid sites is actually changed), the water adsorption on acid sites in the scenario of cofeeding water makes some sites unavailable in the same amount of catalytic bed. Thus, the density of acid sites in the scenario of cofeeding water becomes lower as more water is adsorbed on acid sites. The effect of lowering the density of acid sites explains the slowdown in the kinetic and deactivation in the MTH reaction and the preferential formation of olefins as retained species. The behavior observed in this work is comparable with other strategies to change the density of acid sites in the catalyst such as modifications with metal cations that promote the increase of Lewis acid sites in detriment of Bronsted acid sites [43,62] or the variation in the Si/Al ratio in the zeolite.[63–65] Our results further prove that the olefin cycle (olefins are favored as retained species as shown in our FTIR spectroscopic analysis) would be promoted by the addition of water in the feed for the reason of lowering the density of acid sites, as demonstrated in other works where the density of acid sites is modified by other means.[62,66]

To analyze further the results of the in situ UV-vis cell reactor, we calculated and compared the initial rates of formation and growth of the UV-vis bands:

$$r_i = \left.\frac{dI_i}{dt}\right]_0 \quad (8)$$

Where I represents the intensity of each band (i) measured in the 250-850 nm region of the UV-vis spectrum. This methodology holds because we are using differential conditions where the formation and growth of species are incipient and the concentration of reactants, retained species and products in the reaction media, including the catalysts, is relatively low. In order to compare the net effect of water, we calculated the extent of water quenching as (for $F_{W0}/F_{M0} = R_W = 0.5$):

$$\frac{[r_i]_{R_W=0.5}}{[r_i]_{R_W=0}} = \frac{[r_i]_{0.5}}{[r_i]_0} \quad (9)$$

Figure 10 represent the extent of water quenching for F_{W0}/F_{M0} = 0.5 and 1.0 for all bands and wavelengths (*i*). The important orientation to this figure is the following: a value of 0 indicates that water totally kills the rate of formation and growth of this particular band, a value of 1 indicates that the rate is unaffected by water, a value 0-1 indicates that water is quenching the rate whereas values above 1 indicate that water accelerates the rate. As seen, the rates of formation and growth of all bands decrease by the presence of water, being between 0.50 and 0.84. However, the extent of this quenching is selective: in the range 250-350 nm, all bands decrease ca. 40%, the band at 392 nm only is quenched ca. 20%, whereas the bands of coke of 708 nm can be quenched by water as much as 50%. Additionally, the effect of increasing the amount of water is negligible in the range 250-350 nm but increase for more developed coke species (708 nm). The extent of water quenching is more severe for deactivating species than that of the active species, although the difference is relatively low. This may imply that most of the active species detected in the range of 250-350 nm are olefin species whose formation is favored at increasing water-to-methanol ratios in the feed. Extending the methodology developed here to other catalyst and a wider range of water in the reaction media can provide with optimum values of water fed in order to quench more selectively the deactivation than the reaction.

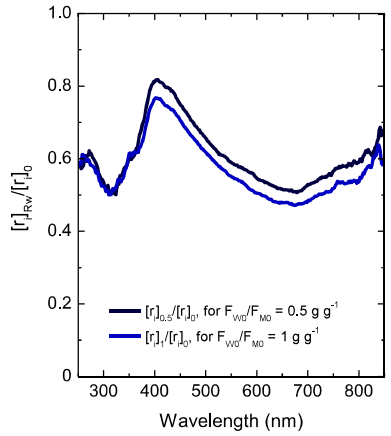

Figure 10. Effect of cofeeding on the extent of water quenching of retained species detected in the whole UV-vis spectrum.

In this work, we further studied how the acid sites are affected by the adsorption of cofed water by using FTIR spectroscopy. Our results indicate that all the acid sites are affected to some extent during the MTH reaction, and particularly, the coverage of silanol sites decreases with increasing water-to-methanol ratios in the feed. The coverage of acid sites occurs by the adsorption of several species. Typically, the interaction of methanol or dimethyl ether with ZSM-5 catalysts gives rise to three types of methoxy species adsorbed on Bronsted, silanol and extra-framework aluminol sites, respectively.[67–69] Likewise, Thibault-Starzyk et al.[70] observed the coke formation on the silanol sites in ZSM-5 catalysts, particularly those located in the zeolite channels. Many authors[71–74] have proved that these sites actively participate in the MTH reaction while also promote deactivation, particularly those in framework defects. Our results reveal that cofeeding water delays the formation and adsorption of deactivating species on these sites, contributing to the prolongation of the catalyst lifetime.

Conclusions

We studied the effect of cofeeding water in the methanol-to-hydrocarbon reaction over a ZSM-5 catalyst using three reaction setups involving fixed-bed and in situ spectroscopic cell reactors. The intention was to analyze the net effect of water on the selective quenching of deactivation (growth of coke) against the formation of active hydrocarbon species on the catalyst. We measured the evolution of retained species by means of extraction and in situ FTIR and UV-vis spectroscopic measurements.

At integral reactor conditions, cofeeding water lowers the conversion due to the coadsorption of water making a portion of acid sites unavailable for the reaction (comparable with decreasing the density of acid sites) that depends on the water-to-methanol ratio in the feed. This effect is comparable with that of changing the space time, in which the decrease of acid sites by decreasing the space time lowers the conversion. A more detailed analysis based on the attenuated kinetic and deactivation coefficients lead to conclude that water attenuates more effectively the deactivation than the reaction. However, at high concentrations of water this effect is reversed due to the saturation of acid sites by water.

At differential reaction conditions, the combined analysis of conversion and the dynamics of retained species (with in situ spectroscopic techniques) lead to conclude that the kinetics of formation and growth of retained species are slowed down by the addition of water in the feed. Importantly, the extent of this quenching depends on the type of retained species. In fact, the rate of coke formation and growth is slowed down more than that of the active hydrocarbon pool species and more at higher amounts of added water. The formation of olefins as retained species is favored when water is cofed, and those the cycle based on olefins is favored.

This work indicates that there is a positive outcome of cofeeding water to the ZSM-5 zeolite during the methanol-to-hydrocarbon reaction because it quenches more the deactivation than the reaction. The methodology developed in this work opens up the opportunity to explore more process variables (such as partial pressures and catalyst) in order to obtain a general view of the effect of water together with the optimized process parameters that enable to take the maximum advantage of cofeeding water.

Author Contributions

José Valecillos, Investigation, Data curation, Formal Analysis, Visualization, Writing – original draft, Writing – review & editing; **Gorka Elordi**, Validation, Writing – review & editing; **Andrés T. Aguayo**, Conceptualization, Formal Analysis, Resources; **Pedro Castaño**, Conceptualization, Funding acquisition, Project administration, Resources, Supervision, Writing – review & editing.

Conflicts of interest

There are no conflicts to declare.

Acknowledgements

This work was possible thanks to the financial support of the Ministry of Economy, Industry and Competitiveness of the Spanish Government (Project CTQ2016-79646-P, co-founded with ERDF funds) and the Basque Government (Project IT748-13, IT912-16). J.V. is thankful for his fellowship granted by the Ministry of Economy, Industry and Competitiveness of the Spanish Government (BES-2014-069980). The authors are thankful for technical and human support provided by IZO-SGI SGIker of UPV/EHU and European funding (ERDF and ESF).

Notes and references

1 U. Olsbye, S. Svelle, M. Bjrgen, P. Beato, T. V. W. Janssens, F. Joensen, S. Bordiga and K. P. Lillerud, *Angew. Chemie - Int. Ed.*, 2012, **51**, 5810–5831.

2 M. Stöcker, *Microporous Mesoporous Mater.*, 1999, **29**, 3–48.

3 I. Yarulina, A. D. Chowdhury, F. Meirer, B. M. Weckhuysen and J. Gascon, *Nat. Catal.*, 2018, **1**, 398–411.

4 C. Wang, J. Xu, G. Qi, Y. Gong, W. Wang, P. Gao, Q. Wang, N. Feng, X. Liu and F. Deng, *J. Catal.*, 2015, **332**, 127–137.

5 M. Bjørgen, U. Olsbye, D. Petersen and S. Kolboe, *J. Catal.*, 2004, **221**, 1–10.

6 I. M. Hill, S. A. Hashimi and A. Bhan, *J. Catal.*, 2012, **285**, 115–123.

7 R. Khare and A. Bhan, *J. Catal.*, 2015, **329**, 218–228.

8 I. M. Dahl and S. Kolboe, *J. Catal.*, 1994, **149**, 458–464.

9 M. Bjørgen, S. Svelle, F. Joensen, J. Nerlov, S. Kolboe, F. Bonino, L. Palumbo, S. Bordiga and U. Olsbye, *J. Catal.*, 2007, **249**, 195–207.

10 A. D. Chowdhury, K. Houben, G. T. Whiting, M. Mokhtar, A. M. Asiri, S. A. Al-Thabaiti, S. N. Basahel, M. Baldus and B. M. Weckhuysen, *Angew. Chemie - Int. Ed.*, 2016, **55**, 15840–15845.

11 Y. Liu, F. M. Kirchberger, S. Müller, M. Eder, M. Tonigold, M. Sanchez-Sanchez and J. A. Lercher, *Nat. Commun.*, 2019, **10**, 1–9.

12 S. Ilias and A. Bhan, *ACS Catal.*, 2013, **3**, 18–31.

13 M. Bjørgen, U. Olsbye and S. Kolboe, *J. Catal.*, 2003, **215**, 30–44.

14 S. Lee and M. Choi, *J. Catal.*, 2019, **375**, 183–192.

15 S. Gao, S. Xu, Y. Wei, Q. Qiao, Z. Xu, X. Wu, M. Zhang, Y. He, S. Xu and Z. Liu, *J. Catal.*, 2018, **367**, 306–314.

16 P. Tian, Y. Wei, M. Ye and Z. Liu, *ACS Catal.*, 2015, **5**, 1922–1938.

17 Y. Wang and F. Wei, in *Multiphase Reactor Engineering for Clean and Low-Carbon Energy Applications*, eds. Y. Cheng, F. Wei and Y. Jin, John Wiley & Sons, Inc., Hoboken, NJ, USA, 2017, pp. 271–294.

18 M. Stöcker, in *Zeolites and Catalysis*, Wiley-VCH Verlag GmbH & Co. KGaA, Weinheim, Germany, 2010, vol. 2, pp. 687–711.

19 A. G. Gayubo, A. T. Aguayo, A. Atutxa, R. Prieto and J. Bilbao, *Ind. Eng. Chem. Res.*, 2004, **43**, 5042–5048.

20 U. Olsbye, S. Svelle, K. P. Lillerud, Z. H. Wei, Y. Y. Chen, J. F. Li, J. G. Wang and W. B. Fan, *Chem. Soc. Rev.*, 2015, **44**, 7155–7176.

21 J. Valecillos, H. Manzano, A. T. Aguayo, J. Bilbao and P. Castaño, *ChemCatChem*, 2019, 5444–5456.

22 M. Shahda, Y. Dengchao and W. Huixin, *Pet. Sci. Technol.*, 2008, **26**, 1893–1903.

23 X. Wu and R. G. Anthony, *Appl. Catal. A Gen.*, 2001, **218**, 241–250.

24 A. J. Marchi and G. F. Froment, *Appl. Catal.*, 1991, **71**, 139–152.

25 M. Ghavipour, R. M. Behbahani, G. R. Moradi and A. Soleimanimehr, *Fuel*, 2013, **113**, 310–317.

26 A. G. Gayubo, A. T. Aguayo, A. L. Morán, M. Olazar and J. Bilbao, *AIChE J.*, 2002, **48**, 1561–1571.

27 K. Chen, A. Gumidyala, M. Abdolrhamani, C. Villines, S. Crossley and J. L. White, *J. Catal.*, 2017, **351**, 130–135.

28 A. G. Gayubo, A. T. Aguayo, M. Castilla, A. L. Morán and J. Bilbao, *Chem. Eng. Commun.*, 2004, **191**, 944–967.

29 K. Chen, J. Damron, C. Pearson, D. Resasco, L. Zhang and J. L. White, *ACS Catal.*, 2014, **4**, 3039–3044.

30 T. I. Batova, E. K. Khivrich, G. N. Shirobokova, N. V. Kolesnichenko, Y. V Pavlyuk and G. N. Bondarenko, *Pet. Chem.*, 2013, **53**, 383–387.

31 W. Song, H. Fu and J. F. Haw, *J. Am. Chem. Soc.*, 2001, **123**, 4749–4754.

32 J. Gil-Coba, S. C. Marie-Rose and J. M. Lavoie, *Catal. Letters*, 2016, **146**, 2534–2542.

33 K. P. Möller, W. Böhringer, A. E. Schnitzler, E. Van Steen and C. T. O'Connor, *Microporous Mesoporous Mater.*, 1999, **29**, 127–144.

34 X. Zhao, J. Li, P. Tian, L. Wang, X. Li, S. Lin, X. Guo and Z. Liu, *ACS Catal.*, 2019, **9**, 3017–3025.

35 A. T. Aguayo, A. G. Gayubo, J. M. Ortega, M. Olazar and J. Bilbao, *Catal. Today*, 1997, **37**, 239–248.

36 K. De Wispelaere, C. S. Wondergem, B. Ensing, K. Hemelsoet, E. J. Meijer, B. M. Weckhuysen, V. Van Speybroeck and J. Ruiz-Martínez, *ACS Catal.*, 2016, **6**, 1991–2002.

37 G. Qi, Z. Xie, W. Yang, S. Zhong, H. Liu, C. Zhang and Q. Chen, *Fuel Process. Technol.*, 2007, **88**, 437–441.

38 F. Rieck genannt Best, A. Mundstock, G. Dräger, P. Rusch, N. C. Bigall, H. Richter and J. Caro, *ChemCatChem*, 2020, **12**, 273–280.

39 M. Luo, Y. Fu, B. Hu, D. Wang, B. Wang and G. Mao, *Appl. Catal. A Gen.*, 2019, **570**, 209–217.

40 F. Schüth, M. D. Ward and J. M. Buriak, *Chem. Mater.*, 2018, **30**, 3599–3600.

41 S. L. Scott, *ACS Catal.*, 2018, **8**, 8597–8599.

42 B. L. Foley, B. A. Johnson and A. Bhan, *ACS Catal.*, 2019, **9**, 7065–7072.

43 J. Valecillos, E. Epelde, J. Albo, A. T. Aguayo, J. Bilbao and P. Castaño, *Catal. Today*, 2019, **348**, 243–256.

44 X. Niu, J. Gao, Q. Miao, M. Dong, G. Wang, W. Fan, Z. Qin and J. Wang, *Microporous Mesoporous Mater.*, 2014, **197**, 252–261.

45 Z. Wei, L. Chen, Q. Cao, Z. Wen, Z. Zhou, Y. Xu and X. Zhu, *Fuel Process. Technol.*, 2017, **162**, 66–77.

46 Y. Bi, Y. Wang, X. Chen, Z. Yu and L. Xu, *Chinese J. Catal.*, 2014, **35**, 1740–1751.

47 W. Wu, W. Guo, W. Xiao and M. Luo, *Fuel Process. Technol.*, 2013, **108**, 19–24.

48 P. Castaño, J. Ruiz-Martínez, E. Epelde, A. G. Gayubo and B. M. Weckhuysen, *ChemCatChem*, 2013, **5**, 2827–2831.

49 D. Mores, E. Stavitski, M. H. F. Kox, J. Kornatowski, U. Olsbye and B. M. Weckhuysen, *Chem. - A Eur. J.*, 2008, **14**, 11320–11327.

50 E. Borodina, H. Sharbini Harun Kamaluddin, F. Meirer, M. Mokhtar, A. M. Asiri, S. A. Al-Thabaiti, S. N. Basahel, J. Ruiz-Martinez and B. M. Weckhuysen, *ACS Catal.*, 2017, **7**, 5268–5281.

51 E. Borodina, F. Meirer, I. Lezcano-González, M. Mokhtar, A. M. Asiri, S. A. Al-Thabaiti, S. N. Basahel, J. Ruiz-Martinez and B. M. Weckhuysen, *ACS Catal.*, 2015, **5**, 992–1003.

52 D. Mores, J. Kornatowski, U. Olsbye and B. M. Weckhuysen, *Chem. - A Eur. J.*, 2011, **17**, 2874–2884.

53 M. Bjørgen, F. Bonino, B. Arstad, S. Kolboe, K. P. Lillerud, A. Zecchina and S. Bordiga, *ChemPhysChem*, 2005, **6**, 232–235.

54 E. D. Hernandez and F. C. Jentoft, , DOI:10.1021/acscatal.0c00721.

55 P. Bollini, T. T. Chen, M. Neurock and A. Bhan, *Catal. Sci. Technol.*, 2019, **9**, 4374–4383.

56 A. Mehdad, N. Gould, B. Xu and R. Lobo, *Catal. Sci. Technol.*, 2017, **8**, 358–366.

57 J. W. Park and G. Seo, *Appl. Catal. A Gen.*, 2009, **356**, 180–188.

58 I. B. Minova, S. K. Matam, A. Greenaway, C. R. A. Catlow, M. D. Frogley, G. Cinque, P. A. Wright and R. F. Howe, *ACS Catal.*, 2019, **9**, 6564–6570.

59 E. Tabor, M. Bernauer, B. Wichterlová and J. Dedecek, *Catal. Sci. Technol.*, 2019, **9**, 4262–4275.

60 S. K. Matam, R. F. Howe, A. Thetford and C. R. A. Catlow, *Chem. Commun.*, 2018, **54**, 12875–12878.

61 A. T. Aguayo, D. Mier, A. G. Gayubo, M. Gamero and J. Bilbao, *Ind. Eng. Chem. Res.*, 2010, **49**, 12371–12378.

62 I. Yarulina, S. Bailleul, A. Pustovarenko, J. R. Martinez, K. De Wispelaere, J. Hajek, B. M. Weckhuysen, K. Houben, M. Baldus, V. Van Speybroeck, F. Kapteijn and J. Gascon, *ChemCatChem*, 2016, **8**, 3057–3063.

63 S. Müller, Y. Liu, F. M. Kirchberger, M. Tonigold, M. Sanchez-Sanchez and J. A. Lercher, *J. Am. Chem. Soc.*, 2016, **138**, 15994–16003.

64 P. Pérez-Uriarte, M. Gamero, A. Ateka, M. Díaz, A. T. Aguayo and J. Bilbao, *Ind. Eng. Chem. Res.*, 2016, **55**, 1513–1521.

65 S. M. T. Almutairi, B. Mezari, E. A. Pidko, P. C. M. M. Magusin and E. J. M. Hensen, *J. Catal.*, 2013, **307**, 194–203.

66 S. Bailleul, I. Yarulina, A. E. J. Hoffman, A. Dokania, E. Abou-Hamad, A. D. Chowdhury, G. Pieters, J. Hajek, K. De Wispelaere, M. Waroquier, J. Gascon and V. Van Speybroeck, *J. Am. Chem. Soc.*, 2019, **141**, 14823–14842.

67 X. Z. Jiang, *J. Mol. Catal. A Chem.*, 1997, **121**, 63–68.

68 T. R. Forester and R. F. Howe, *J. Am. Chem. Soc.*, 1987, **109**, 5076–5082.

69 Saepurahman, M. Visur, U. Olsbye, M. Bjørgen and S. Svelle, *Top. Catal.*, 2011, **54**, 1293–1301.

70 F. Thibault-Starzyk, A. Vimont, C. Fernandez and J. P. Gilson, *Chem. Commun.*, 2000, **70**, 1003–1004.

71 X. Meng, M. Zhang, C. Chen, C. Li, W. Xiong and M. Li, *Appl. Catal. A Gen.*, 2018, **558**, 122–130.

72 P. Sazama, B. Wichterlova, J. Dedecek, Z. Tvaruzkova, Z. Musilova, L. Palumbo, S. Sklenak and O. Gonsiorova, *Microporous Mesoporous Mater.*, 2011, **143**, 87–96.

73 K. Barbera, F. Bonino, S. Bordiga, T. V. W. Janssens and P. Beato, *J. Catal.*, 2011, **280**, 196–205.

74 M. Grahn, A. Faisal, O. G. W. Öhrman, M. Zhou, M. Signorile, V. Crocellà, M. S. Nabavi and J. Hedlund, *Catal. Today*, 2020, **345**, 136–146.